

---

# OPTIMIZING CONVOLUTIONAL NEURAL NETWORKS FOR CHRONIC OBSTRUCTIVE PULMONARY DISEASE DETECTION IN CLINICAL COMPUTED TOMOGRAPHY IMAGING

---

A PREPRINT

✉ Tina Dorosti<sup>1-3</sup>, Manuel Schultheiss<sup>1-3</sup>, Felix Hofmann<sup>3</sup>, Johannes Thalhammer<sup>1-4</sup>,  
Luisa Kirchner<sup>3</sup>, Theresa Urban<sup>1-3</sup>, Franz Pfeiffer<sup>1-4</sup>,  
Florian Schaff<sup>1,2</sup>, Tobias Lasser<sup>2,5</sup>, Daniela Pfeiffer<sup>3-4</sup>

1 Chair of Biomedical Physics, Department of Physics, School of Natural Sciences

2 Munich Institute of Biomedical Engineering

3 Department of Diagnostic and Interventional Radiology, School of Medicine, Klinikum rechts der Isar

4 Institute for Advanced Study

5 Computational Imaging and Inverse Problems, Department of Computer Science, School of Computation, Information, and Technology

Technical University of Munich, Germany

✉ tina.dorosti@tum.de

## Summary statement:

Manual versus automated window-setting optimization for computed tomography images was explored, and binary detection of chronic obstructive pulmonary disease was improved with a DenseNet when input data was preprocessed to the emphysema window setting.

## Key points:

1. Manual preprocessing of CT images to emphysema window setting improved binary detection of chronic obstructive pulmonary disease with various CNNs.
2. DenseNet achieved a significantly better mean area under the Receiver Operating Characteristics curve at 0.86 when provided with input data preprocessed to the emphysema window setting compared to data without any window setting preprocessing ( $P=0.03$ ).
3. By automating the window-setting optimization process through the addition of a customized layer to the DenseNet, optimal window settings in the proximity of the emphysema window setting were learned.

**Keywords** CT images · CNN · emphysema · optimization · window setting

**Abbreviations:** Area Under Receiver Operating Characteristics Curve (AUC), Convolutional Neural Network (CNN), Chronic Obstructive Pulmonary Disease (COPD), Computed Tomography (CT), Densely Connected CNN (DenseNet), Hounsfield Unit (HU), Receiver Operating Characteristics (ROC), Window Level (WL), Window-Setting Optimization (WSO), Window Width (WW)

## ABSTRACT

**Purpose:** To optimize the binary detection of Chronic Obstructive Pulmonary Disease (COPD) based on emphysema presence in the lung with convolutional neural networks (CNN) by exploring manually adjusted versus automated window-setting optimization (WSO) on computed tomography (CT) images.

**Methods:** 7,194 CT images (3,597 with COPD; 3,597 healthy controls) from 78 subjects (43 with COPD; 35 healthy controls) were selected retrospectively (10.2018 – 12.2019) and preprocessed. For each image, intensity values were manually clipped to the emphysema window setting and a baseline ‘full-range’ window setting. Class-balanced train, validation, and test sets contained 3,392, 1,114, and 2,688 images. The network backbone was optimized by comparing various CNN architectures. Furthermore, automated WSO was implemented by adding a customized layer to the model. The image-level area under the Receiver Operating Characteristics curve (AUC) [lower, upper limit 95% confidence] and  $P$ -values calculated from one-sided Mann-Whitney U-test were utilized to compare model variations.

**Results:** Repeated inference ( $n=7$ ) on the test set showed that the DenseNet was the most efficient backbone and achieved a mean AUC of 0.80 [0.76, 0.85] without WSO. Comparably, with input images manually adjusted to the emphysema window, the DenseNet model predicted COPD with a mean AUC of 0.86 [0.82, 0.89] ( $P=0.03$ ). By adding a customized WSO layer to the DenseNet, an optimal window in the proximity of the emphysema window setting was learned automatically, and a mean AUC of 0.82 [0.78, 0.86] was achieved.

**Conclusion:** Detection of COPD with DenseNet models was improved by WSO of CT data to the emphysema window setting range.

## 1 Introduction

Chronic Obstructive Pulmonary Disease (COPD) is a group of respiratory diseases impairing the lung structure, such as emphysema [1]. With 3.23 million deaths recorded globally in 2019, COPD is among the leading causes of death worldwide [2]. In addition to increased mortality rates directly correlating with the disease, patients with COPD preconditions are at a higher risk for all-cause mortality [3][4][5]. With early detection and intervention, COPD's prevalence and negative impacts can be decreased [3].

Spirometry is a readily available pulmonary function test for COPD detection and is often utilized to categorize the disease progression into four stages (GOLD I-IV) [1]. Although spirometry reliably detects advanced stages of COPD, false negative results dominate in the early stages [1][6]. Moreover, patients diagnosed with COPD at the same GOLD stage have shown drastic morphological differences in the lung structure [7].

Alternatively, COPD is detected with an X-ray Computed Tomography (CT) scan, where detailed three-dimensional morphological information about the lung structure is obtained in Hounsfield Unit (HU) values. This information on phenotypic abnormalities and patterns of morphological changes reflecting emphysema allows for detecting and controlling disease progression even in the early stages. In 2015, the Fleischner Society introduced a disease progression scale based on the pattern of abnormalities in CT data corresponding to COPD and emphysema subtypes [7].

In recent years, increasing large-scale COPD studies [8][9] in parallel with advancing machine learning models have made Convolutional Neural Networks (CNNs) a popular tool for binary classification of COPD [10][11][12][13][14]. Despite their promising results, these models are still not ready for integration into a computer-aided clinical workflow for efficient COPD diagnosis. CNN research in other medical imaging tasks has demonstrated the benefits of incorporating clinically-relevant steps in the model workflow. In particular, optimizing window-setting parameters of input CT images can improve the results [15][16][17]. However, implementing preprocessing steps to adapt clinical workflow processes has yet to be explicitly explored in the extant literature on COPD detection with CNNs.

We hypothesize that COPD detection with CNN models can be improved by adapting preprocessing based on existing radiological knowledge, specifically through window-setting optimization (WSO). In this exploratory study, we aim to optimize the binary detection of COPD based on emphysema presence in the lung with CNNs by exploring the effects of manually adjusted versus automated WSO on CT images.

## 2 Methods

### 2.1 Dataset

7,194 CT images from 78 subjects were selected retrospectively (10.2018 – 12.2019), as shown in Figure 1. Approval from an ethics committee and patient informed consent were obtained. CT scans included subjects suffering from COPD (n=43, images=3,597) and healthy controls (n=35, images=3,597), previously reported as a sub-cohort of this X-ray dark-field chest radiography study [18]. The CT scans were first anonymized and then graded by three expert radiologists with 4 – 12 years of experience based on the Fleischner Score categories of centrilobular emphysema [7]. Scans with scores greater than ‘mild’ were considered as the COPD class for the binary classification task. Scans with ‘moderate’ scores were further annotated on image-level by another radiologist (FH) to distinguish images presenting COPD. Datasets were class-balanced and selected on image level: Train, validation, and test sets included 3,392; 1,114; and 2,688 images, respectively. Patient demographics for each set are given in Table 1.

### 2.2 Data preprocessing

Each image was segmented to the lung region, clipped to the respective window setting, and normalized. Window settings are given by the window width and level (WW, WL) HU. The emphysema window (124, -962) HU was used to clip the CT images for the classification of COPD. Furthermore, a ‘full-range’ windowing (2048, 0) HU, selected based on the minimum and the maximum intensity values recorded over all images, was considered the baseline window setting. Figure 2 shows examples of images from both classes preprocessed to the full-range and the emphysema windows. It can be observed that emphysematous patches of low attenuation have more contrast in the images preprocessed to the emphysema window.

<sup>1</sup>Note. Age is given in terms of each set’s mean and age range [youngest, oldest].

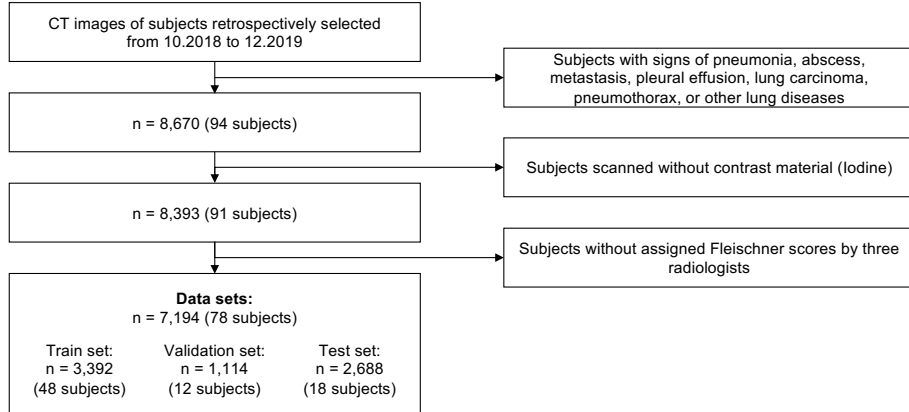


Figure 1: Flowchart describing the data selection process. 7,194 CT images from our clinic were selected retrospectively and anonymized for the binary classification of Chronic Obstructive Pulmonary Disease (COPD).

Table 1: Subject Demographics (n = 78)

Parameter \subset	Train		Validation		Test	
	No COPD	COPD	No COPD	COPD	No COPD	COPD
Male	21	5	6	1	10	5
Female	20	2	4	1	3	0
Age <sup>1</sup> (years)	62.7 [34, 91]	70.3 [55, 80]	63.9 [49, 80]	71.0 [70, 72]	64.9 [31, 77]	75.2 [65, 83]

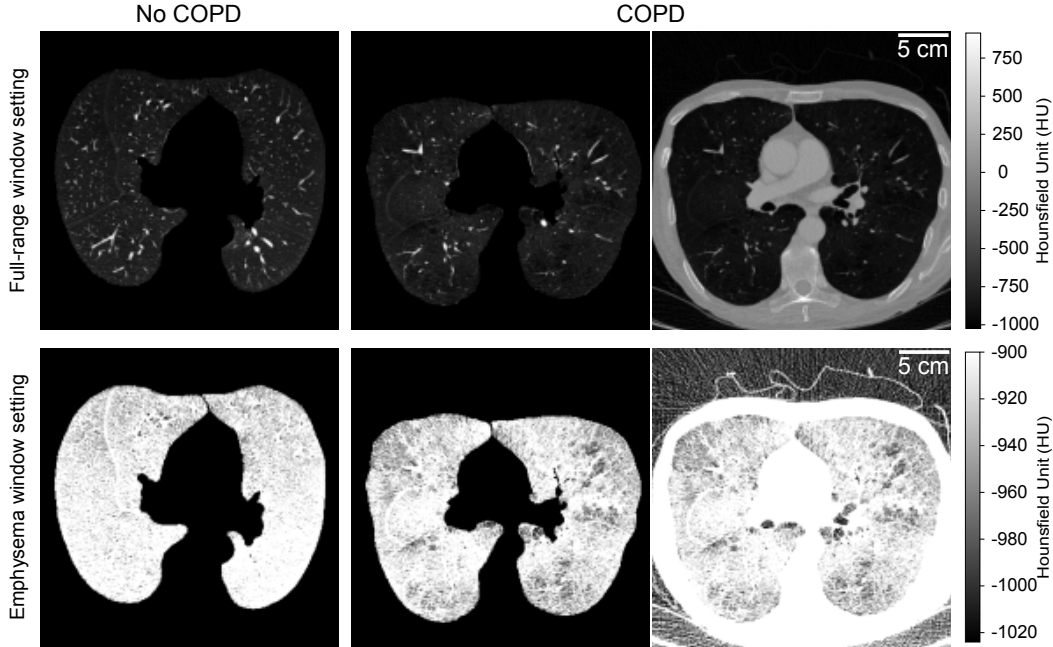


Figure 2: Example images from the Chronic Obstructive Pulmonary Disease (COPD) and no COPD class preprocessed to full-range and emphysema window settings. The no COPD image is segmented to the lung region and corresponds to a healthy subject. The COPD image is shown in both segmented and original form and corresponds to a subject with a Fleischner score of ‘advanced’ centrilobular emphysema. The nonhomogeneous patches of low attenuation corresponding to emphysema are more contrasted in the emphysema-clipped image. All images include a contrast medium (Iodine).

## 2.3 Network Architectures

All models were implemented in TensorFlow (2.4.0) [19] and compiled with binary cross entropy loss and the Adam optimizer [20]. Reducing the learning rate by a factor of ten and early stopping were scheduled over 15 and 50 epochs, respectively, if the validation loss did not decrease.

### 2.3.1 Backbone Comparison

To select the model with the best performance and efficiency, DenseNet-121, EfficientNetV2-M, and ResNet-34 architectures were examined [21][22][23]. The models were trained and tested on images linearly clipped to the full-range and the emphysema window settings to analyze the influence of the window-setting preprocessing on binary COPD detection. Based on the results presented in Table 2 and section 3.1, DenseNet-121 (plain DenseNet) was chosen as the backbone architecture. Figure 3 details the selected DenseNet architecture.

### 2.3.2 DenseNet<sub>WSO</sub>

A WSO layer was added to the plain DenseNet, as suggested by [16], to create DenseNet<sub>WSO</sub>. Here, only the ReLU activation function is considered for the WSO layer, as it consistently outperformed the sigmoid variant. Therefore, the WSO layer depicted in Figure 3 consisted of a 1x1 convolution layer followed by a ReLU activation. The ReLU acted as a windowing function and was trained to find an optimal window setting for the detection task. The WW and WL values related to the learnable weight (w) and bias (b) parameters of the ReLU function, taken from [16] with correction,

$$f_{\text{ReLU}}(x) = \max(\min(wx + b, U), 0), \quad \text{where } w = \frac{U}{WW}, \quad b = \frac{U}{WW} \left( \frac{WW}{2} - WL \right). \quad (1)$$

The upper bound for the ReLU windowing function, U=1, was set to achieve learned window settings ranging between zero and one. The DenseNet<sub>WSO</sub> model was trained to converge to an optimal window setting after initialization to either the full-range or the emphysema window settings while simultaneously adjusting learnable parameters of the DenseNet block for the detection task. Initialization of the WSO layer was carried out by defining the learnable parameters for each window setting respectively. All input images for DenseNet<sub>WSO</sub> were given in the full-range window and normalized. The optimal window settings learned by the model were calculated with (1).

### 2.3.3 DenseNet<sub>FNF</sub>

To stabilize the learned window setting over all runs, the DenseNet<sub>WSO</sub> model was first trained with the learnable parameters from the WSO layer frozen and fixed to the initialized settings. Then, the model was further trained with the unfrozen WSO layer, which allowed its parameters to adjust for the optimal window setting. The same model was also trained continuously for a third round with the learnable parameters of the WSO layer frozen. This training sequence with frozen, not frozen, and frozen (FNF) WSO layer learnable parameters is called DenseNet<sub>FNF</sub>.

## 2.4 Saliency Maps

The gradient of the class score with respect to the input image was calculated to generate the saliency maps [24].

## 2.5 Evaluation Metrics

Models were initialized randomly and trained from scratch for seven runs; each model run was inferred once with the test data. The Receiver Operating Characteristics (ROC) curve and the area under the ROC curve (AUC) were used to assess the models' performance. Utilizing different threshold choices, the AUC alleviates the ambiguity regarding maximizing sensitivity or (1 - specificity) for smaller sample sizes [25]. The Scikit-learn library (1.2.0) was used to generate the ROC curves, choose optimal thresholds for each curve, and calculate the respective AUC values [26]. 95% confidence intervals (CI) [lower limit,upper limit] and *P*-values from one-sided Mann-Whitney U-test were calculated with SciPy library (1.4.1) [27][28].

## 3 Results

This section presents the binary COPD detection results of the backbone comparison and the three DenseNet variants on the test set's 2,688 images. External public datasets were not considered because they use the GOLD progression scale rather than the Fleischner score as ground truth labels.

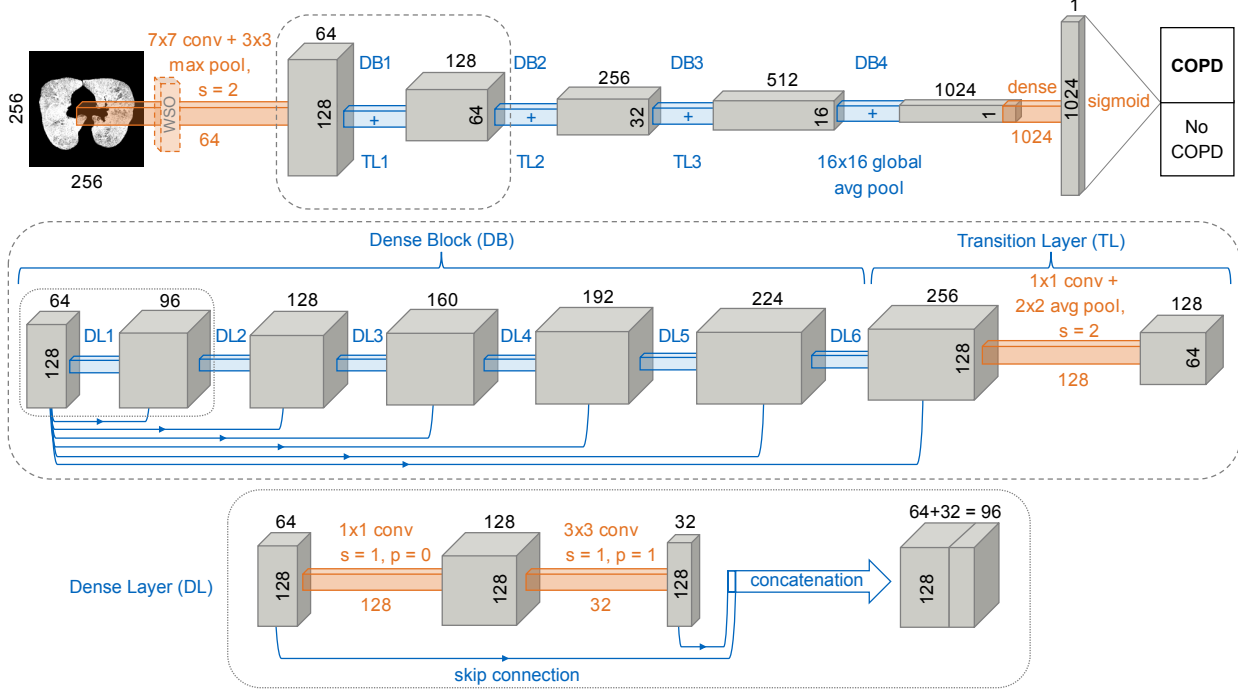


Figure 3: DenseNet architecture with 121 layers used for binary classification of Chronic Obstructive Pulmonary Disease (COPD). The model constituents, Dense Block (DB), Dense Layer (DL), and Transition Layer (TL), are expanded in detail. The convolution (conv) and pooling (pool) layers are described by their stride (s) and padding (p) parameters. DenseNet-characteristic skip connections are shown in the DB and DL. The model had a growth rate of 32. The window-setting optimization (WSO) layer consisted of a 1x1 convolution layer followed by a Rectified Linear Unit (ReLU) activation and was used for the automatic optimization of the window settings in the DenseNet<sub>WSO</sub> and DenseNet<sub>FNF</sub> implementations. The architecturally specific vertical digits for each box represent the side length dimensions, and the numbers over each block correspond to the number of filters.

### 3.1 Backbone Architecture and Manual WSO

Table 2 provides the AUC values for the architectural backbone comparison on the test set over seven runs. Preprocessing the input data to the emphysema window significantly improved the model performance for the EfficientNetV2-M ( $P = 0.006$ ) and DenseNet-121 ( $P = 0.03$ ). Overall, EfficientNetV2-M and DenseNet-121 showed higher AUC values compared to ResNet-34. Preprocessing the input images to the full-range window resulted in a mean  $AUC = 0.80$  for both EfficientNetV2-M and DenseNet-121, with the DenseNet-121 presenting a comparatively narrower 95% CI. For input images preprocessed to the emphysema window setting, EfficientNetV2-M outperformed DenseNet-121 by a mean AUC difference of 0.03. Regarding computational efficiency, ResNet-34 and EfficientNetV2-M had an approximate mean training time of 90 minutes per run, whereas DenseNet-121 had a mean training time of roughly 30 minutes per run. Consequently, DenseNet-121 (plain DenseNet) was chosen as the backbone architecture for the task at hand.

Table 2: Area Under the Receiver Operating Characteristics Curve (AUC) for Backbone Architecture Comparison (n=7)

Model \ window setting	Mean AUC		AUC 95% Confidence Interval	
	Full-range	Emphysema	Full-range	Emphysema
ResNet-34	0.75	0.79 ( $P = 0.06$ )	[0.70, 0.80]	[0.74, 0.84]
EfficientNetV2-M	0.80	0.89 ( $P = 0.006$ )	[0.71, 0.90]	[0.87, 0.91]
DenseNet-121 (plain DenseNet)	0.80	0.86 ( $P = 0.03$ )	[0.76, 0.85]	[0.82, 0.89]

Using the plain DenseNet model, image-level ROC plots with corresponding AUC values were compared between full-range and emphysema window settings in the top row of Figure 4. Since the test set had balanced images from both classes of no COPD and COPD, the chance diagonal was used as a visual guide to mark the AUC value of 0.5. Plain DenseNet results in Figure 4 show that clipping data to the emphysema window setting consistently results in

significantly higher values (mean AUC = 0.86 [0.82, 0.89]) in comparison to the full-range window setting (mean AUC = 0.80 [0.76, 0.85]) ( $P=0.03$ ). Among all plain DenseNet results, the last model run, with the input images preprocessed to the emphysema window setting, led to the highest AUC value of 0.91.

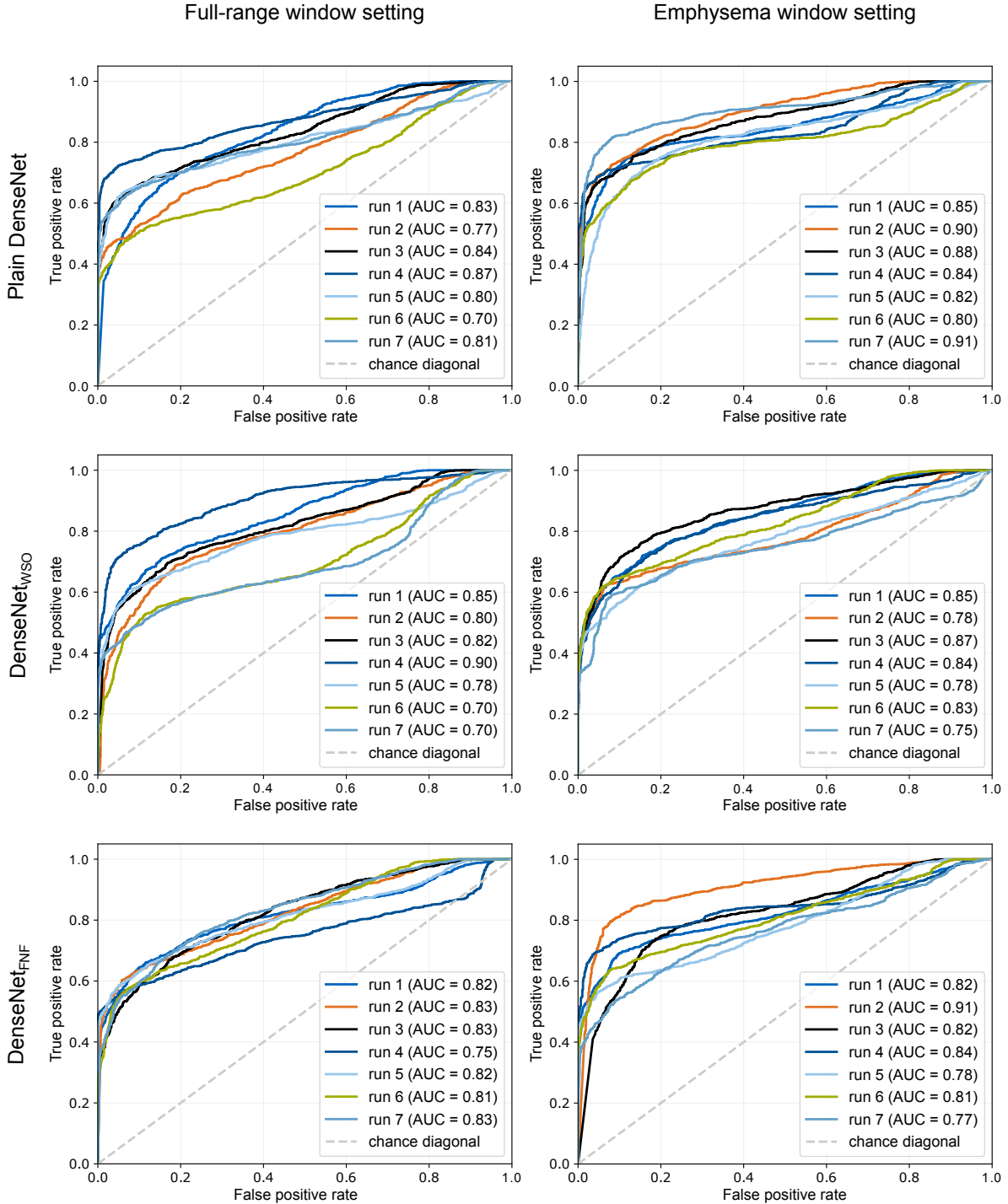


Figure 4: The Receiver Operating Characteristics (ROC) curve and the area under the ROC curve (AUC) results. Inference on 2,688 image-level test data preprocessed to full-range and emphysema window settings shown for each run of the three model variants, plain DenseNet, DenseNetwso, and DenseNet<sub>FNF</sub>.

### 3.2 Automatic WSO

The window-setting values in Table 3 correspond to the mean and 95% CI values for WW and WL over the seven runs of each arrangement. The information in Table 3 is independent of the inference data set, as the learned window-setting values are fixed model-specific parameters after a completed training run. The learned WW and WL parameters were calculated from the weights and bias values of the WSO layer using (1). Figure 5 shows the learned and the corresponding initialization window setting for each WSO model. Note that the window settings used for the initialization of WSO models were the same as the parameters used for preprocessing the inputs to the plain DenseNet.

Table 3: Standard and Learned Window Setting by DenseNet Variants (n=7)

Model \ window setting	Full-range (Width, Level) HU	Emphysema (Width, Level) HU
Standard (Plain DenseNet)	(2048, 0)	(124, -962)
Learned (DenseNet <sub>WSO</sub> )	(1301 [676, 1927], -373 [-686, -61])	(90 [79, 102], -979 [-985, -973])
Learned (DenseNet <sub>FNF</sub> )	(993 [681, 1305], -528 [-684, -372])	(114 [79, 148], -967 [-984, -950])

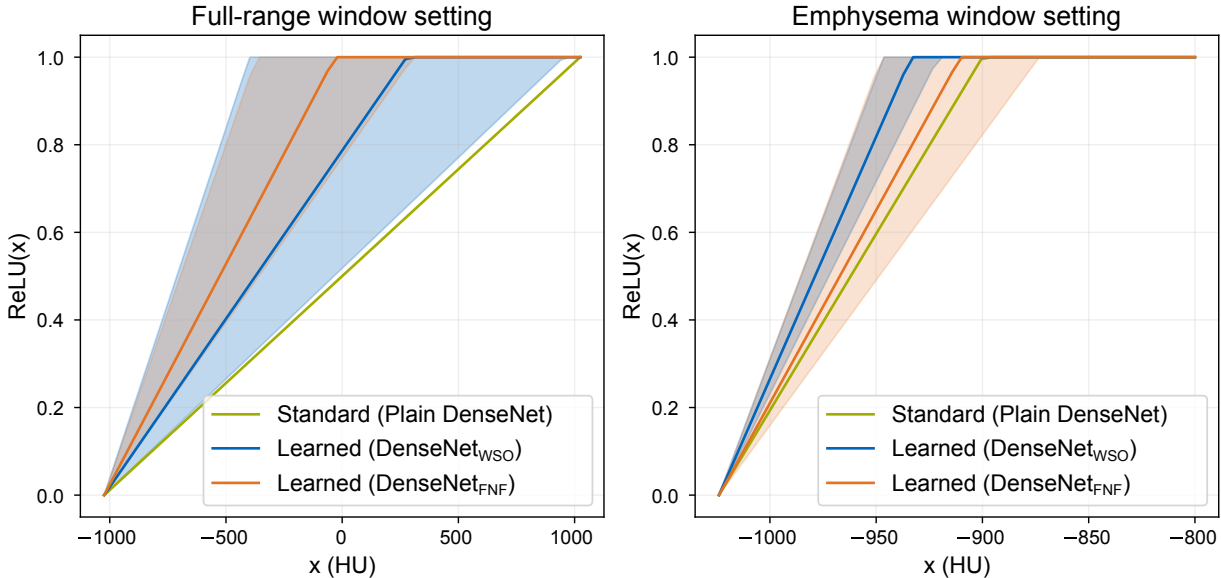


Figure 5: Learned window settings with 95% confidence intervals (CI). Standard full-range and emphysema window settings (green) are plotted against the mean learned window setting with 95% CI over seven runs for DenseNet<sub>WSO</sub> (blue) and DenseNet<sub>FNF</sub> (orange). Note that the standard window settings were used to preprocess the inputs for the plain DenseNet and to initialize the DenseNet<sub>WSO</sub> and DenseNet<sub>FNF</sub>. The exact values for window settings are provided in Table 3.

A shift towards the lower end of the HU range in all learned window settings is noticeable, as given in Table 3 and Figure 5. The mean learned WL decreased more drastically for models initialized to the full-range window setting. The observed trends suggest a convergence towards the standard emphysema window setting for the learned WW and WL parameters by DenseNet<sub>WSO</sub> and DenseNet<sub>FNF</sub> when initialized to the full-range window setting. Between the two models, DenseNet<sub>FNF</sub> learned a window setting closer to the emphysema window setting regardless of the initialization window setting. However, when initialized to the full-range window, the DenseNet<sub>FNF</sub> arrived at the mean WW and WL parameters over seven runs with less deviation than when the model was initialized to the emphysema window. Overall, better mean AUC values are achieved when the learned window setting is closer to the standard emphysema window.

Figure 4 depicts the ROC curves for DenseNet<sub>WSO</sub> and DenseNet<sub>FNF</sub> models in the bottom rows. Initialization to emphysema windowing results in more consistent AUC values over seven runs compared to the full-range window setting for the DenseNet<sub>WSO</sub> model. Conversely, for the DenseNet<sub>FNF</sub> model, initialization to the full-range window generates more consistent AUC values over seven runs compared to the emphysema window setting. These results agree with the 95% CI values given in Table 3 and Figure 5. The highest AUC value achieved between the DenseNet<sub>WSO</sub> and the DenseNet<sub>FNF</sub> models was 0.91. This corresponded to the second run of the emphysema window setting initialization for the DenseNet<sub>FNF</sub> model.

Evaluating this specific model run with the test set, given a classification threshold at 0.5, the resulting values are true negative (TN) = 1,171, false negative (FN) = 218, true positive (TP) = 1,126, and false positive (FP) = 173. Example images in both the learned and the standard emphysema windows for the TP, TN, FP, and FN cases and their corresponding saliency-map overlays are provided in Figure 6. The weights are well spread out over both lung lobes for the TN case. In contrast, for the FP case, the weights are focused on a region with minimal drop in HU values, falsely categorizing a non-existent emphysema pattern. The emphysematous patches of low attenuation correctly emphasized in the TP case are not recognized as such in the FN case, specifically in the right lobe. The learned window setting for this specific model, (162, -943) HU, has a slightly higher level and wider width compared to the standard emphysema window setting, contributing to the more contrasted images.

### 3.3 Optimal Window Setting

The mean AUC values for all model and window setting combinations for inference on the test set are provided in Table 4. Taking the plain DenseNet model with full-range input images as the baseline, the plain DenseNet with input images initialized to the emphysema window setting resulted in the best mean AUC value at 0.86 [0.82, 0.89] ( $P=0.03$ ). Implementing the WSO layer in DenseNet<sub>WSO</sub> and DenseNet<sub>FNF</sub> models did not significantly enhance the AUC compared to the results obtained with the plain DenseNet. Compared to the baseline, the DenseNet<sub>FNF</sub> model generated slightly better AUC values when initialized to either window setting. However, the most optimal window setting for the COPD detection task was the standard emphysema window setting of (124, -962) HU and not a window setting learned by either of the automated WSO models.

Table 4: Area Under the Receiver Operating Characteristics Curve (AUC) for DenseNet Variant Comparison (n=7)

Model \window setting	Mean AUC		AUC 95% Confidence Interval	
	Full-range	Emphysema	Full-range	Emphysema
Plain DenseNet	0.80	0.86 ( $P^2 = 0.03$ )	[0.76, 0.85]	[0.82, 0.89]
DenseNet <sub>WSO</sub>	0.79	0.81 ( $P = 0.40$ )	[0.73, 0.86]	[0.78, 0.85]
DenseNet <sub>FNF</sub>	0.81	0.82 ( $P = 0.36$ )	[0.79, 0.83]	[0.78, 0.86]

## 4 Discussion

We explored manually adjusted versus automated WSO for CT images with CNNs to optimize the binary detection of COPD. Manual preprocessing of CT images to emphysema window setting consistently improved binary detection of COPD with various CNNs. Specifically, DenseNet efficiently achieved a significantly better mean AUC=0.86 [0.82, 0.89] when provided with input data preprocessed to the emphysema window setting compared to data preprocessed to the full-range window setting ( $P = 0.03$ ). Furthermore, optimal window settings in the proximity of the emphysema window setting were learned by automating the window-setting optimization process through the addition of a customized layer to the DenseNet. Our findings demonstrate that diligent preprocessing based on existing radiological knowledge and selecting phenotypically representative ground truth labels positively impacts the outcome of COPD detection with CNN models.

Three CNN architectures were examined based on their characteristics and existing results in literature: ResNets and DenseNets benefit from skip connections, improving the gradient stability and information flow throughout the network [21][23]. Furthermore, both models have shown promising results in COPD classification [13][14]. EfficientNets were also considered as they require less computing and promise fast training [22]. Although the results show the best mean AUCs for EfficientNetV2-M, DenseNet-121 achieved comparable mean AUCs with a shorter mean training time.

We showed that adjusting input images to different window settings directly impacts the binary detection of COPD; preprocessing CT images to the emphysema window consistently improves the performance of EfficientNetV2-M, ResNet-34, and DenseNet-121 models on the binary detection of COPD. Taking the AUC values for the plain DenseNet model with full-range input data as the baseline, when the input was preprocessed to the emphysema window, the AUC values increased from 0.80 to 0.86. The AUC values for the DenseNet<sub>WSO</sub> model suggest the shortcoming of the model in simultaneously detecting COPD and converging to optimal windowing parameters when initialized to the full-range window setting. Furthermore, the windowing parameters learned with this setup suffered from large deviations across the seven runs as evidenced by the wide 95% CIs. Narrower 95% CIs in learned window settings were observed when

<sup>2</sup>Note.  $P$ -values for each model/setting combination are calculated with respect to the baseline of plain DenseNet for full-range input data.

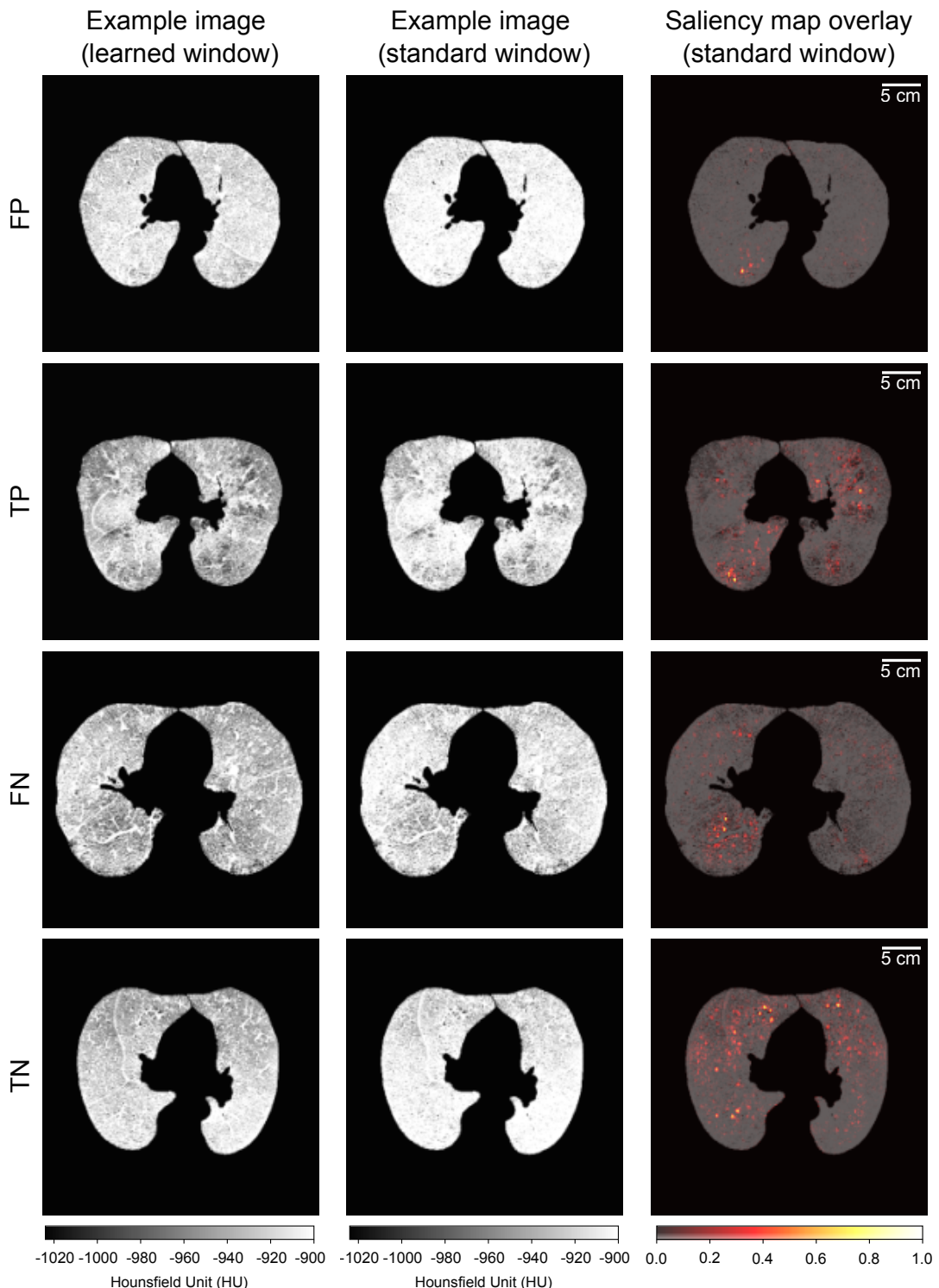


Figure 6: Example images for case analysis. The true negative (TN), false negative (FN), true positive (TP), and false positive (FP) cases are shown for the best model run from the DenseNet<sub>FNF</sub> initialized to the emphysema window setting (area under the curve = 0.91, classification threshold = 0.5). Images for each case are shown in the window setting learned by the model (162, -943) HU and the standard emphysema window setting (124, -962) HU. For each case, the overlay of the saliency map and the image in the standard emphysema window is provided to explain the model performance. All images include a contrast medium (Iodine).

the WSO layer was trained with periodically frozen learnable parameters, as implemented in DenseNet<sub>FNF</sub> initialized to the full-range window setting.

Through automatic WSO, only minimal improvement in AUC value was observed with the DenseNet<sub>WSO</sub> and the DenseNet<sub>FNF</sub> models initialized to emphysema window setting, compared to the baseline. The window settings learned by these two models were in the vicinity of the standard emphysema window at the lower ranges of the HU scale. However, neither DenseNet<sub>WSO</sub> nor DenseNet<sub>FNF</sub> outperformed the plain DenseNet model with images preprocessed to the standard emphysema window setting. A possible explanation is that although the single WSO layer converged to the optimal emphysema window setting, it was not sufficiently complex for optimal window setting selection. Nonetheless, if information regarding the optimal window setting for the detection of COPD is unknown, learning an optimal windowing by adding a WSO layer with the DenseNet<sub>FNF</sub> model results in higher AUC values in comparison to training a plain DenseNet model with full-range normalized images.

The standard emphysema windowing is tailored to present high contrast between healthy and emphysematous lung tissues. Therefore, as the ground truth labels for our dataset were graded based on the severity of emphysema, the results were in line with the hypothesis that images clipped directly to the standard emphysema windowing or automatically clipped with the WSO layer to a learned window-setting in the proximity of standard emphysema window, would improve detection of COPD with DenseNets. Optimizing for window setting to increase contrast in images was effective for the detection task because the Fleischner Score ground-truth labels were directly based on disease-relevant morphological changes in the lung. Therefore, adjusting input data based on window settings may be less effective for models trained with spirometry-based GOLD standard COPD stages as ground truth labels for lung CTs. Utilizing the Fleischner Score as ground-truth labels also enabled us to achieve comparable results to related works in the literature, despite using a smaller dataset [11][12][13][14].

The main limitation of this work was its relatively small dataset, giving rise to intra-image correlation for image-level evaluations. Additionally, all subjects were examined at the same hospital. The extendibility of our findings to a larger, more diverse dataset should be further explored. In the context of COPD, future works could further explore the categorical classification of the disease based on the progression scale introduced by the Fleischner Society.

We showed that optimizing for a task-specific window-setting improved CNN outcome by enhancing disease-relevant information from the input data. Our findings can be extended to a range of computer vision tasks in medicine, focusing on X-ray and CT data. By incorporating disease-relevant window settings commonly used by radiologists into the deep learning pipeline, the performance of models can be improved.

## Acknowledgments

This work was funded by the Federal Ministry of Education and Research (BMBF) and the Free State of Bavaria under the Excellence Strategy of the Federal Government and the Länder, the German Research Foundation (GRK2274), as well as by the Technical University of Munich–Institute for Advanced Study.

## References

- [1] C. F. Vogelmeier *et al.*, “Global Strategy for the Diagnosis, Management, and Prevention of Chronic Obstructive Lung Disease 2017 Report. GOLD Executive Summary,” *Am. J. Resp. Crit. Care. Med.*., vol. 195, no. 5, pp. 557–582, Mar. 2017. Accessed on: Aug. 17, 2022, DOI: 10.1164/RCCM.201701-0218PP, [Online].
- [2] World Health Organization. (2022, May. 20). *Fact sheets: Chronic Obstructive Pulmonary Disease (COPD)*. Geneva, Switzerland. May 20, 2022. [Online]. Available: [https://www.who.int/en/news-room/fact-sheets/detail/chronic-obstructive-pulmonary-disease-\(copd\)](https://www.who.int/en/news-room/fact-sheets/detail/chronic-obstructive-pulmonary-disease-(copd)). Accessed on: Aug. 18, 2022.
- [3] D. M. Mannino and S. Braman, “The epidemiology and economics of chronic obstructive pulmonary disease,” in *Proc. Am. Thorac. Soc.*., vol. 4, no. 7, pp. 502–506, Oct. 2007, Accessed on: Aug. 17, 2022, DOI: 10.1513/pats.200701-001FM, [Online].
- [4] Q. Zhao *et al.*, “The impact of COPD and smoking history on the severity of COVID-19: A systemic review and meta-analysis,” *J. Med. Virol.*., vol. 92, no. 10, pp. 1915–1921, Oct. 2020. Accessed on: Aug. 17, 2022, DOI: 10.1002/JMV.25889, [Online].
- [5] D. M. G. Halpin *et al.*, “Global Initiative for the Diagnosis, Management, and Prevention of Chronic Obstructive Lung Disease. The 2020 GOLD Science Committee Report on COVID-19 and Chronic Obstructive Pulmonary Disease ,” *Am. J. Resp. Crit. Care. Med.*., vol. 203, no. 1, pp. 24–36, Jan. 2021. Accessed on: Aug. 18, 2022, DOI: 10.1164/RCCM.202009-3533SO, [Online].

[6] P. A. Grenier. "Emphysema at CT in Smokers with Normal Spirometry: Why It Is Clinically Significant," *Radiology*., vol. 296, no. 3, pp. 650–651, Jul. 2020. Accessed on: Aug. 18, 2022, DOI: 10.1148/RADIOL.2020202576, [Online].

[7] D. A. Lynch *et al.*, "CT-Definable Subtypes of Chronic Obstructive Pulmonary Disease: A Statement of the Fleischner Society," *Radiology*., vol. 277, no. 1, pp. 192–205, Oct. 2015. Accessed on: Aug. 18, 2022, DOI: 10.1148/radiol.2015141579, [Online].

[8] E. A. Regan *et al.*, "Genetic epidemiology of COPD (COPDGene) study design," *COPD*., vol. 7, no. 1, pp. 32–43, Feb. 2010. Accessed on: Aug. 18, 2022, DOI: 10.3109/15412550903499522, [Online].

[9] J. Vestbo *et al.*, "Evaluation of COPD Longitudinally to Identify Predictive Surrogate End-points (ECLIPSE)," *Eur. Respir. J.*., vol. 31, no. 4, pp. 869–873, Apr. 2008. Accessed on: Aug. 18, 2022, DOI: 10.1183/09031936.00111707, [Online].

[10] Y. Lecun, Y. Bengio, and G. Hinton, "Deep learning," *Nature*., vol. 521, no. 7553, pp. 436–444, May 2015. Accessed on: Aug. 18, 2022, DOI: 10.1038/nature14539, [Online].

[11] T. T. Ho *et al.*, "A 3D-CNN model with CT-based parametric response mapping for classifying COPD subjects," *Sci. Rep.*., vol. 11, no. 1, pp. 1–12, Jan. 2021. Accessed on: Aug. 18, 2022, DOI: 10.1038/s41598-020-79336-5, [Online].

[12] G. Gonzalez *et al.*, "Disease Staging and Prognosis in Smokers Using Deep Learning in Chest Computed Tomography," *Am. J. Resp. Crit. Care. Med.*., vol. 197, no. 2, pp. 193–203, Jan. 2018. Accessed on: Aug. 18, 2022, DOI: 10.1164/RCCM.201705-0860OC., [Online].

[13] L. Y. W. Tang, H. O. Coxson, S. Lam, J. Leipsic, R. C. Tam, and D. D. Sin, "Towards large-scale case-finding: training and validation of residual networks for detection of chronic obstructive pulmonary disease using low-dose CT," *Lancet Digit. Health.*., vol. 2, no. 5, pp. e259–e267, May 2020. Accessed on: Aug. 18, 2022, DOI: 10.1016/S2589-7500(20)30064-9, [Online].

[14] L. Zhang, B. Jiang, H. J. Wisselink, R. Vliegenthart, and X. Xie, "COPD identification and grading based on deep learning of lung parenchyma and bronchial wall in chest CT images," *Br. J. Radiol.*., vol. 95, no. 1133, May 2022. Accessed on: Feb. 03, 2023, DOI: 10.1259/bjr.20210637, [Online].

[15] M. Kloenne *et al.*, "Domain-specific cues improve robustness of deep learning-based segmentation of CT volumes," *Sci. Rep.*., vol. 10, no. 1, pp. 1–9, Jul. 2020. Accessed on: Aug. 18, 2022, DOI: 10.1038/s41598-020-67544-y, [Online].

[16] H. Lee, M. Kim, and S. Do, "Practical window setting optimization for medical image deep learning." Presented at *NIPS*, Dec. 2018. [Online]. Available: <https://arxiv.org/abs/1812.00572>.

[17] X. Wang *et al.*, "A deep learning algorithm for automatic detection and classification of acute intracranial hemorrhages in head CT scans," *Neuroimage. Clin.*., vol. 32, pp. 1–10, Jan. 2021, Accessed on: Aug. 18, 2022, DOI: 10.1016/J.NICL.2021.102785, [Online].

[18] T. Urban *et al.*, "Qualitative and Quantitative Assessment of Emphysema Using Dark-Field Chest Radiography," *Radiology*., vol. 303, no. 1, pp. 119–127, Jan. 2022. Accessed on: Jul. 27, 2023, DOI: 10.1148/radiol.212025, [Online].

[19] M. Abadi *et al.*, "TensorFlow: Large-Scale Machine Learning on Heterogeneous Systems," 2015. Accessed on: Aug. 29, 2022, Available: <https://www.tensorflow.org/>, [Online].

[20] D. P. Kingma and J. L. Ba, "Adam: A Method for Stochastic Optimization." Presented at *ICLR*, Dec. 2015. [Online]. Available: <https://arxiv.org/abs/1412.6980>.

[21] G. Huang, Z. Liu, L. Van Der Maaten, and K. Q. Weinberger, "Densely Connected Convolutional Networks," in *Proc. IEEE CVPR*, Honolulu, HI, USA, 2017, pp. 2261–2269.

[22] M. Tan, and Q. V. Le, "EfficientNetV2: Smaller Models and Faster Training." Presented at *ICML*, 2021. [Online]. Available: <https://arxiv.org/abs/2104.00298>.

[23] K. He, X. Zhang, S. Ren, and J. Sun, "Deep Residual Learning for Image Recognition." *ArXiv*, 2015. [Online]. Available: <https://arxiv.org/abs/1512.03385>.

[24] K. Simonyan, A. Vedaldi, and A. Zisserman, "Deep inside convolutional networks: Visualising image classification models and saliency maps," 2nd International Conference on Learning Representations, *ICLR* 2014 - Workshop Track Proceedings. 2014.

[25] D. P. Chakraborty, "Modeling the binary task," in *Observer Performance Methods for Diagnostic Imaging*. Boca Raton, FL, USA: CRC Press, 2021, ch. 3, sec. 9 – 12, pp. 47–57.

- [26] F. Pedregosa *et al.*, “Scikit-learn: Machine Learning in Python,” *JMLR.*, vol. 12, pp. 2825–2830, 2011. Accessed on: Aug. 29, 2022, Available: <https://scikit-learn.org/>, [Online].
- [27] P. Virtanen et al., “SciPy 1.0: Fundamental Algorithms for Scientific Computing in Python,” *Nat Methods.* 2020; 17(3): 261-272. doi: 10.1038/s41592-019-0686-2.
- [28] H.B. Mann, D.R. Whitney. “On a Test of Whether one of Two Random Variables is Stochastically Larger than the Other”. *Ann. Math. Statist.* 1947 Mar; 18 (1) 50-60. <https://doi.org/10.1214/aoms/1177730491>.